Applied Catalysis B: Environmental 144 (2014) 41–45

Contents lists available at ScienceDirect

Applied Catalysis B: Environmental

journal homepage: www.elsevier.com/locate/apcatb

Photocatalytic hydrogen production from glycerol and water with NiO_x/TiO_2 catalysts

Ruixia Liu, Hiroshi Yoshida, Shin-ichiro Fujita, Masahiko Arai*

Division of Chemical Process Engineering, Faculty of Engineering, Hokkaido University, Sapporo 060-8628, Japan

ARTICLE INFO

Article history:
Received 18 April 2013
Received in revised form 6 June 2013
Accepted 20 June 2013
Available online 29 June 2013

Keywords:
Photocatalytic activity
Glycerol reforming
Hydrogen production
Nickel doping
Titanium dioxide

ABSTRACT

The surface of a TiO_2 material was modified by loading NiO_x in 10 wt% by impregnation with nickel nitrate followed by calcination in air at different temperatures. The TiO_2 and NiO_x/TiO_2 samples prepared were applied for photocatalytic H_2 production from glycerol and water at 50 °C. The H_2 evolution was enhanced by NiO_x loading and was dependent on calcination temperature. A maximum H_2 evolution was observed with 450 °C calcined NiO_x/TiO_2 sample. The properties of those TiO_2 and NiO_x/TiO_2 samples were characterized by nitrogen adsorption, XRD, UV/vis, and XPS measurements to examine factors responsible for the enhancement of photocatalytic H_2 evolution with NiO_x loaded and calcined TiO_2 samples.

1. Introduction

The useful application of biomass derived materials is attracting much attention from industry and academia. One of interesting applications is the production of H_2 from chemical and photochemical transformations of those materials [1–3]. The photocatalytic H_2 production can be performed under mild conditions and several authors studied different biomass derived model materials including alcohols, glycerol, glucose, sugars, and so on. Recently a larger amount of glycerol is produced as a byproduct in the production of biodiesel and so it is desirable to find its application [4]. The heterogeneous photocatalytic H_2 production from aqueous glycerol solutions (Scheme 1) was studied by several authors using TiO_2 based catalysts loaded with Pt [5–8], Pd [9], and CuO_x [10–12]. Fornasiero et al. prepared active Cu/TiO_2 catalysts by a water-in-oil microemulsion method, in which Cu nanoparticles were embedded in the TiO_2, and these were active for the H_2 production from glycerol and water under visible light irradiation conditions [10]. The doping of NiO_x onto the surface of TiO_2 is effective for the preparation of p-type (NiO_x)–n-type (TiO_2) junction [13]. Such NiO_x-doped TiO_2 catalysts were recently reported to show good performance of photocatalytic degradation of organic compounds of methyl orange [14], methylene blue [15], and 2-naphthol and *p*-cresol [16]. In the present work, the authors prepared NiO_x/TiO_2 catalysts by conventional impregnation and tested their performance in photocatalytic H_2 production from a mixture of glycerol and water under UV/vis irradiation conditions. We could find few published study that has considered the use of NiO_x/TiO_2 photo-sensitive materials for such a H_2 production from biomass derived compounds.

2. Experimental

2.1. Catalyst preparation

A TiO_2 material supplied by Catalysis Society of Japan was used, which was a mixture of anatase and rutile TiO_2. The structural properties will be presented later (Table 1). The doping of Ni species was made by conventional impregnation with nickel nitrate (Wako) and the loading of Ni species was 10% by weight assuming Ni species was in the form of NiO. A weighed TiO_2 (1 g) was dispersed in 10 cm^3 $Ni(NO_3)_2$ aqueous solution (0.15 M) and the slurry formed was continuously stirred overnight for sufficient impregnation. The mixture was kept in an oven at 80 °C for 12 h to remove the solvent (water). Then, the solid sample was ground and calcined in a muffle furnace while passing air at 50 cm^3 min^{-1} at 250, 450 and 650 °C for 3 h. The catalysts so prepared are denoted by NiO_x/TiO_2 hereinafter.

2.2. Catalyst characterization

The surface and bulk properties of NiO_x/TiO_2 samples prepared were characterized by different methods. BET surface area was measured by N_2 adsorption at −196 °C (Quantachrome NOVA 1000). Prior to N_2 physisorption, the samples were degassed under vacuum at 150 °C for 2 h. Structural properties were examined by

* Corresponding author. Tel.: +81 11 7066594; fax: +81 11 7066594.
E-mail address: marai@eng.hokudai.ac.jp (M. Arai).

0926-3373/$ – see front matter © 2013 Elsevier B.V. All rights reserved.
http://dx.doi.org/10.1016/j.apcatb.2013.06.024

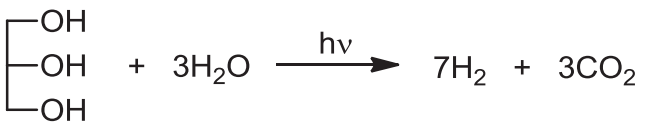

Scheme 1. Photocatalytic reaction between glycerol and water.

powder X-ray diffraction (XRD) (Rigaku D/Max-2500 PC) with Cu Kα radiation and a Ni filter. XRD patterns were measured from 20° to 80° at a rate of 1° min^{-1}. Diffuse reflection UV/vis spectra were recorded under ambient conditions (Shimadzu UV-3100PC) using $BaSO_4$ matrix as background under ambient conditions. The spectra measured were converted to the absorption spectra by using the Kubelka–Munk function. X-ray photoelectron spectroscopy (JEOL JPS-9200) was used to examine the surface properties and all the binding energies were referenced with respect to the Ti 2p at 485.5 eV [17].

2.3. Photocatalytic reaction

Photocatalytic reactions were conducted in the same reactor as used previously, which was a 50 cm^3 stainless steel autoclave with two quartz windows (diameter 1 cm) [18]. It was previously used for photocatalytic water splitting in the presence of pressurized CO_2. A weighed sample (20 mg) was suspended in a mixture of 10 cm^3 water and 2 cm^3 glycerol (Wako) in the reactor. The air remaining in the reactor was removed by purging with 1 MPa N_2 for five times. The reactor was placed on a heating plate and wrapped by a heating tape. The temperature was monitored by a thermocouple embedded in the reactor wall. The reactor was heated while stirring the reaction mixture by a magnetic stirrer. The reaction mixture was illuminated using a 500 W high-pressure Hg lamp (Ushio USH-500SC) at 50 °C for 4 h. The lamp emits predominantly the light of wavelengths at 365 nm, 405 nm, and 436 nm. After the reaction, the gaseous products evolved were collected in a gas trap. The amount of H_2 was determined by a gas chromatograph (Shimadzu GC-8A, molecular sieve 5A packed column, TCD detector, N_2 carrier) and those of CO, CO_2, and CH_4 by another gas chromatograph (Shimadzu GC-8A, Porapak Q packed column, FID detector, N_2 carrier) with a methanizer converting those gases into CH_4.

3. Results and discussion

In the present work, 10 wt% NiO_x/TiO_2 catalysts calcined at different temperatures were used for the photocatalytic H_2 production from aqueous glycerol solution. The 10 wt% NiO loading approximately corresponds to monolayer coverage of NiO species over the surface of TiO_2 used that has a BET surface area of 50 $m^2 g^{-1}$. The state of NiO_x dispersion (namely, the state of NiO_x–TiO_2 junction/contact) was varied by changing the calcination temperature.

Table 1
Structural properties of NiO_x/TiO_2 catalysts determined by N_2 adsorption and XRD measurements.

Catalyst	Anatase/rutile ratio	Crystallite size[a] (nm)			Surface area
		TiO_2	NiO	$NiTiO_3$	($m^2 g^{-1}$)
TiO_2	83/17	21	–	–	50
NiO_x/TiO_2 250 °C[b]	80/20	22	4	–	54
NiO_x/TiO_2 450 °C[b]	80/20	23	6	–	50
NiO_x/TiO_2 650 °C[b]	9/91	27	–	51	14

[a] The average crystallite size of TiO_2 was calculated by following equation: $D_{ave} = D_a \times [I_a/(I_a + I_r)] + D_r \times [I_r/(I_a + I_r)]$, where D_{ave} is average crystallite size and D_a and D_r are crystallite size of anatase $d(1\,0\,1)$ and rutile $d(1\,1\,0)$, respectively. I_a and I_r are the peak intensity of anatase $d(1\,0\,1)$ and rutile $d(1\,1\,0)$, respectively. The ratio of anatase and rutile was determined by the equation $W_r = 1/[1 + 0.8 \times (I_a/I_r)]$ and $W_a = 1 - W_r$, where W_a and W_r are the molar ratio of anatase and rutile. The average crystallite size of NiO and $NiTiO_3$ were calculated by the Scherrer's formula, $D = 0.9 \times \lambda/(\beta_{1/2} \times \cos\theta)$, λ is the wavelength (0.15418 nm Cu K_α radiation) of the X-ray, $\beta_{1/2}$ line-width at medium height of anatase $d(1\,0\,1)$, rutile $d(1\,1\,0)$, NiO $d(2\,0\,0)$ and $NiTiO_3$ $d(1\,0\,4)$, and θ the diffraction angle. For these calculation procedures, see Refs. [22–24].

[b] Calcination temperature.

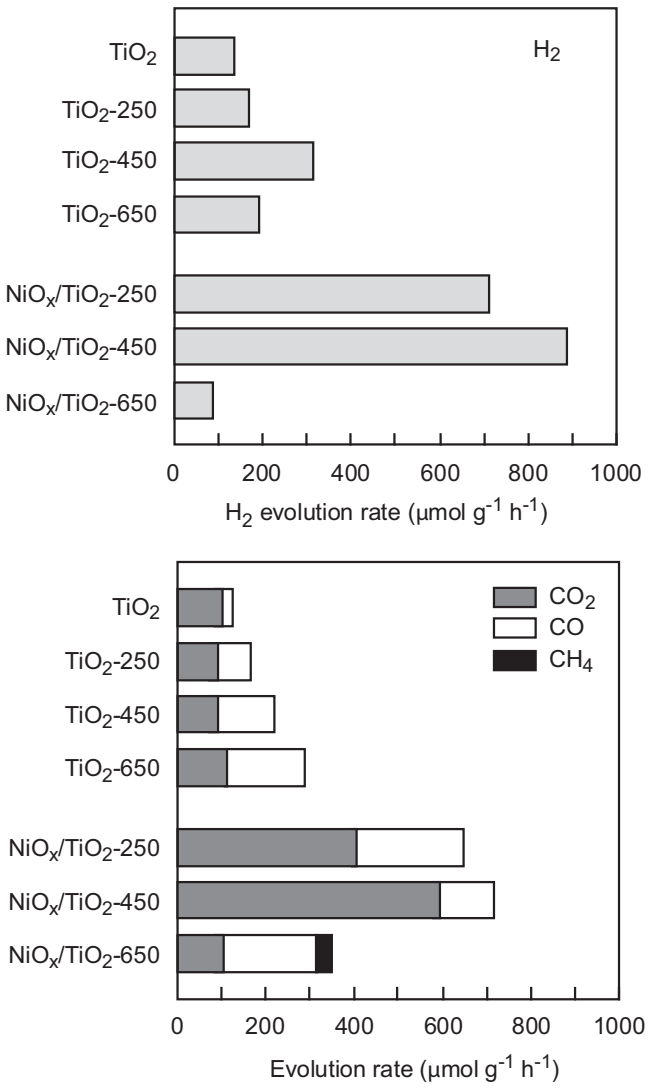

Fig. 1. Evolution of H_2 (upper) and other gaseous products (bottom) in photocatalytic reaction at 50 °C between glycerol and water with NiO_x-unloaded and loaded TiO_2 samples uncalcined and calcined at 250 °C, 450 °C, and 650 °C.

3.1. Catalytic performance

First, the performance of NiO_x-unloaded TiO_2 samples calcined at different temperatures was examined for photocatalytic H_2 production from a mixture of glycerol and water at 50 °C. Fig. 1 shows the rates of evolution of H_2 and other gaseous products of CO_2 and CO in photocatalytic reforming of glycerol at 50 °C. The evolution of CH_4 was not detected. When the calcination temperature was raised, the rate of H_2 evolution increased, had a maximum at 450 °C, and then decreased. The maximum H_2 evolution was 320 μmol g^{-1} h^{-1} under the conditions used. The amount of CO_2 evolved did not change so much but that of CO increased with the temperature. The evolution of H_2 was larger than that of CO_2 and CO for the catalysts calcined at 450 °C or below but smaller for the one at 650 °C. In addition, blank experiments were conducted in

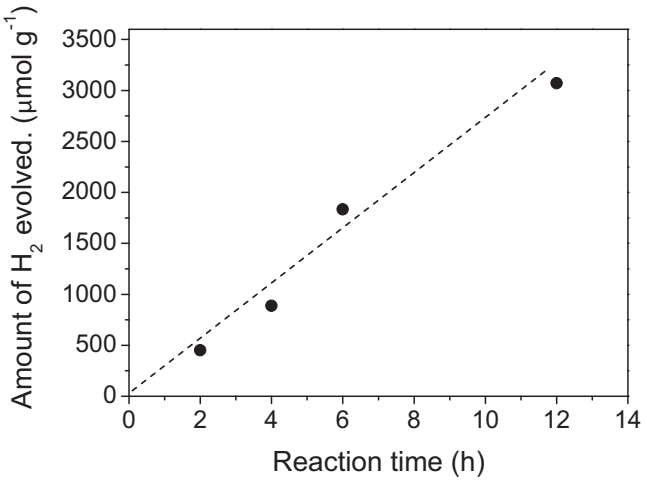

Fig. 2. Time profile of the H_2 evolution in photocatalytic reaction between glycerol and water at 50 °C with NiO_x/TiO_2 catalyst calcined at 450 °C.

the absence of light and/or catalyst under the same reaction conditions. No H_2 production was detected in these blank reactions, indicating that both the light and the TiO_2 catalyst are required for the photocatalytic H_2 production from glycerol and water.

Then, the catalytic performance of NiO_x-loaded TiO_2 samples was tested and the results obtained are also shown in Fig. 1. The rate of H_2 evolution changed with the calcination temperature in a similar manner as observed with the NiO_x-unloaded samples. The maximum H_2 evolution appeared at the same temperature of 450 °C, being 900 μmol g^{-1} h^{-1}. It was about three times larger compared to the maximum with the NiO_x-unloaded sample calcined at 450 °C. Thus, the loading of NiO_x to TiO_2 can improve its photocatalytic performance. The total amount of CO_2 and CO formed was comparable to that of H_2 evolved for either 250 °C or 450 °C calcined NiO_x/TiO_2 catalyst. However, the ratio of CO_2 against CO is different, being 1.8 and 5.4 for the former and latter catalysts, respectively. CH_4 was also detected to form for the 650 °C calcined sample.

In addition, the performance of NiO alone was tested under the same reaction conditions. The NiO powder was prepared by calcining $Ni(NO_3)_2$ at 450 °C in an air stream of 50 cm^3 min^{-1} for 3 h and grinding in a mortar. This treatment changed $Ni(NO_3)_2$ to NiO, which was confirmed by XRD (not shown). It was found that H_2, CO, and CH_4 were evolved at rates of 91, 2124, and 917 μmol g^{-1} h^{-1}, respectively. That is, compared to the above-mentioned NiO_x/TiO_2 sample calcined at the same temperature, the amount of H_2 was even smaller while those of CO and CH_4 were even larger. Hence, reactions with NiO alone are different from those with NiO_x/TiO_2 catalysts and so NiO is not effective for our target H_2 production from aqueous glycerol solution, for which the significance of NiO_x–TiO_2 junction/contact is again illustrated.

Hydrogen could be produced through the two reactions in which one is photo-splitting of water and the other is photo-reforming of glycerol with water (Scheme 1). To examine the significance of the two reactions, the NiO_x/TiO_2 samples calcined at 250 °C, 450 °C, and 650 °C were also tested for the photocatalytic H_2 production from water in the absence of glycerol. The maximum H_2 production was observed to occur for the 450 °C calcined sample. However, it was only 6.6 μmol g^{-1} h^{-1}, which was smaller by two orders of magnitude than that in the presence of glycerol. Hence, for a mixture of glycerol and water, the H_2 was evolved through photocatalytic reaction between the two.

The most active 450 °C calcined catalyst was further tested for longer reaction periods of time. Fig. 2 indicates the time profile obtained, showing that the H_2 production continued to occur at an almost fixed rate during the reaction up to 12 h and so the catalyst did not change in its activity.

In our reaction runs, gas chromatograph analysis was tried to detect possible liquid products of CH_3OH, HCOOH, CH_3OH, and C_2H_5OH. We failed to detect such products, which may be ascribed to low conversion of glycerol (<0.05% estimated rough from the initial amount of glycerol used and the total amount of H_2 evolved in 4 h with the most active catalyst) and/or these should easily be changed to gaseous products by action of NiO.

The photocatalytic production of H_2 from aqueous glycol solution was recently studied over TiO_2 catalysts in the absence of costly noble metals [10–12]. Fornasiero et al. prepared several types of CuO_x/TiO_2 catalysts by different methods and showed that Cu nanoparticle embedded TiO_2 catalysts prepared by a water-in-oil microemulsion method have superior performance compared to conventional Cu/TiO_2 catalysts prepared by impregnation [10,11]. The performance of our NiO_x/TiO_2 catalysts prepared by conventional impregnation is comparable to their Cu/TiO_2 catalysts. Lalitha et al. also studied the performance of CuO_x/TiO_2 catalysts prepared by impregnation and calcination at 350 °C and 450 °C [12].

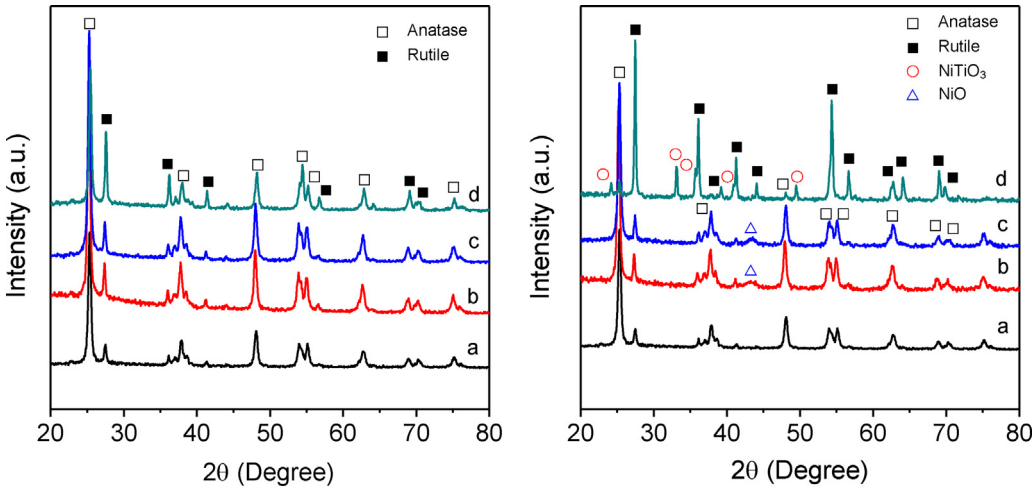

Fig. 3. XRD patterns (left) for NiO_x-unloaded TiO_2 samples untreated (a) and calcined at 250 °C (b), 450 °C (c), and 650 °C (d) and (right) for NiO_x-unloaded (a) and loaded TiO_2 samples calcined at 250 °C (b), 450 °C (c), and 650 °C (d).

The photocatalysts of Fornasiero et al. and Lalitha et al. are visible light sensitive. (Our NiO_x/TiO_2 catalysts have not been tested under visible light conditions due to the limitation of experimental setup.)

3.2. Catalyst characterization

The properties of NiO_x-loaded and unloaded TiO_2 samples calcined at different temperatures were examined by different methods. Table 1 shows the results of N_2 adsorption. The 650 °C calcined sample had a markedly decreased surface area of 14 $m^2\ g^{-1}$. In contrast, the surface area of NiO_x-unloaded TiO_2 was observed to decrease to 43 $m^2\ g^{-1}$, indicating that the significant decrease in the surface area of NiO_x-loaded TiO_2 by the calcination at 650 °C is induced by the doping of NiO_x. Fig. 3 gives XRD patterns and the bulk phase composition and other parameters determined thereof. The anatase/rutile ratio was 83/17 and the size of TiO_2 was 21 nm for NiO_x-unloaded mother TiO_2 sample. These structural parameters did not change by the NiO_x-loading and the following calcination at 250 °C and 450 °C. After the calcination at 650 °C, however, the phase composition changed drastically to an anatase/rutile ratio of 9/91. The phase composition also changed by the calcination for NiO_x-unloaded TiO_2 but less markedly; the anatase/rutile ratio decreased to 59/41 by the calcination at 650 °C. Thus, the phase transformation of TiO_2 during the calcination was assisted by the presence of NiO_x species. The average TiO_2 crystallite size increased with the temperature but marginally. For the NiO_x-loaded samples calcined at 250 °C and 450 °C, NiO was detected, the size being 4–6 nm; NiO was highly dispersed on the surface of TiO_2. On calcination at 650 °C, the NiO changed to $NiTiO_3$ with an average size of 51 nm and the BET surface decreased significantly to 14 $m^2\ g^{-1}$.

Fig. 4 shows UV/vis spectra of those NiO_x-loaded and unloaded TiO_2 samples. The loading of 10 wt% NiO_x was found to have a significant impact on the absorption at wavelength > 350 nm. The NiO_x loading strengthened the absorption in this range of wavelength, depending on the calcination temperature used. These data were reformed to a plot of (absorbance·energy)$^{1/2}$ against energy in Fig. 4(b). For NiO_x-unloaded TiO_2, the band gap was estimated to be 2.75 eV; while, for the NiO_x-loaded samples calcined at 250 °C and 450 °C, it was lowered to 2.17 eV. The difference was 0.58 eV. The decrease in the band gap energy may be one of factors responsible for the enhanced H_2 production rate observed with the 250 °C and 450 °C calcined NiO_x/TiO_2 catalysts (Fig. 1). The band gap of TiO_2 depends on its structure, being 3.2–3.3 eV for anatase TiO_2 [19,21] and 3.0–3.1 eV for rutile TiO_2 [20,21]. In our samples, the phase composition did not change by the loading of NiO_x and the calcination at temperatures of 250 °C and 450 °C (Table 1). Therefore, the decrease in the band gap observed should result from the formation of NiO_x and TiO_2 junction. This desirable N–P junction was likely to be destroyed after the calcination at a higher temperature of 650 °C, at which NiO_x changed to $NiTiO_3$ (Fig. 3).

The catalysts were further characterized by XPS measurements. Fig. 5 shows Ni_{2p}, Ti_{2p}, and O_{1s} XPS spectra collected with the NiO_x unloaded and loaded TiO_2 samples calcined at different temperatures. For the unmodified TiO_2, the binding energy (BE) values of Ti $2p_{3/2}$ and Ti $2p_{1/2}$ were 458.5 eV and 464.5 eV, respectively, the difference being 6 eV. These peaks may come from anatase TiO_2 species and a shoulder peak at 457 eV from rutile TiO_2 species. The loading of NiO_x and the following calcination caused significant changes: the 650 °C calcined sample had a peak at a BE of 464 eV but no other peaks were detected, in which the surface Ti species should be in a structure different from anatase and rutile TiO_2 species. The 450 °C calcined sample also had a peak at a similar BE along with a small peak at about 457 eV. The latter peak indicated that a small amount of Ti species of rutile structure remained on its surface. The 250 °C calcined may be on a way of changing from a

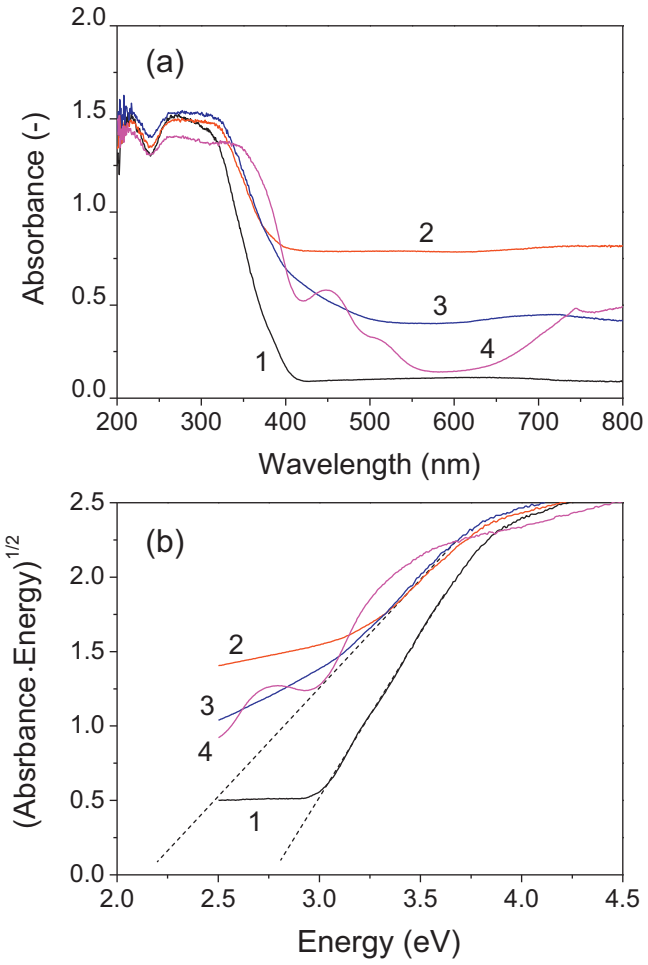

Fig. 4. (a) UV/vis spectra measured for NiO_x-unloaded (1) and loaded TiO_2 samples calcined at different temperatures of 250 °C (2), 450 °C (3), and 650 °C (4). (b) Plot of (absorbance·energy)$^{1/2}$ against energy obtained from the data (a).

mixture of anatase and rutile Ti species to other structures. A similar significant change was observed for O 1s. The NiO_x-unloaded TiO_2 sample had a peak at 529.5 eV while the 450 °C and 650 °C calcined ones had a peak at a larger BE of 535 eV. According to the literature, the BE values of NiO and Ni_2O_3 are 529.7 eV and 531.5 eV, respectively. The spectra of Ni 2p were a little noisy but the peaks were detected at 860 eV and 865 eV. The BE values of Ni $2p_{3/2}$ of metallic Ni, NiO, $NiAl_2O_3$, and $NiWO_4$ are 852.3 eV, 853.3 eV, 857.2 eV, and 857.6 eV, respectively, [17], which are smaller compared to the peaks observed with the NiO_x-loaded calcined TiO_2 samples. At present, unfortunately, it is difficult to determine the surface Ni–Ti–O structure but it may be assumed that the above-mentioned NiO_x–TiO_2 junction was formed for the calcined NiO_x/TiO_2 samples. Very recently Iwaszuki et al. investigated the performance of NiO_x-loaded TiO_2 catalysts for the photocatalytic degradation of 2-naphthol and *p*-cresol and discussed their high performance after considering their structural features estimated theoretically by density functional theory simulations [16]. It is assumed that NiO clusters have a strong interaction with the surfaces of anatase and rutile TiO_2 through Ni—O—Ti bonds and additional Ni—Ti bonds for rutile TiO_2. These structural changes caused by NiO loading can reduce the band gap energy.

Hence, it can be said that the loading of NiO_x onto TiO_2 and the following calcination cause the bang gap energy to lower by 2.5 eV and this is one of factors responsible for the enhancement of the photocatalytic activity in H_2 production from glycerol and

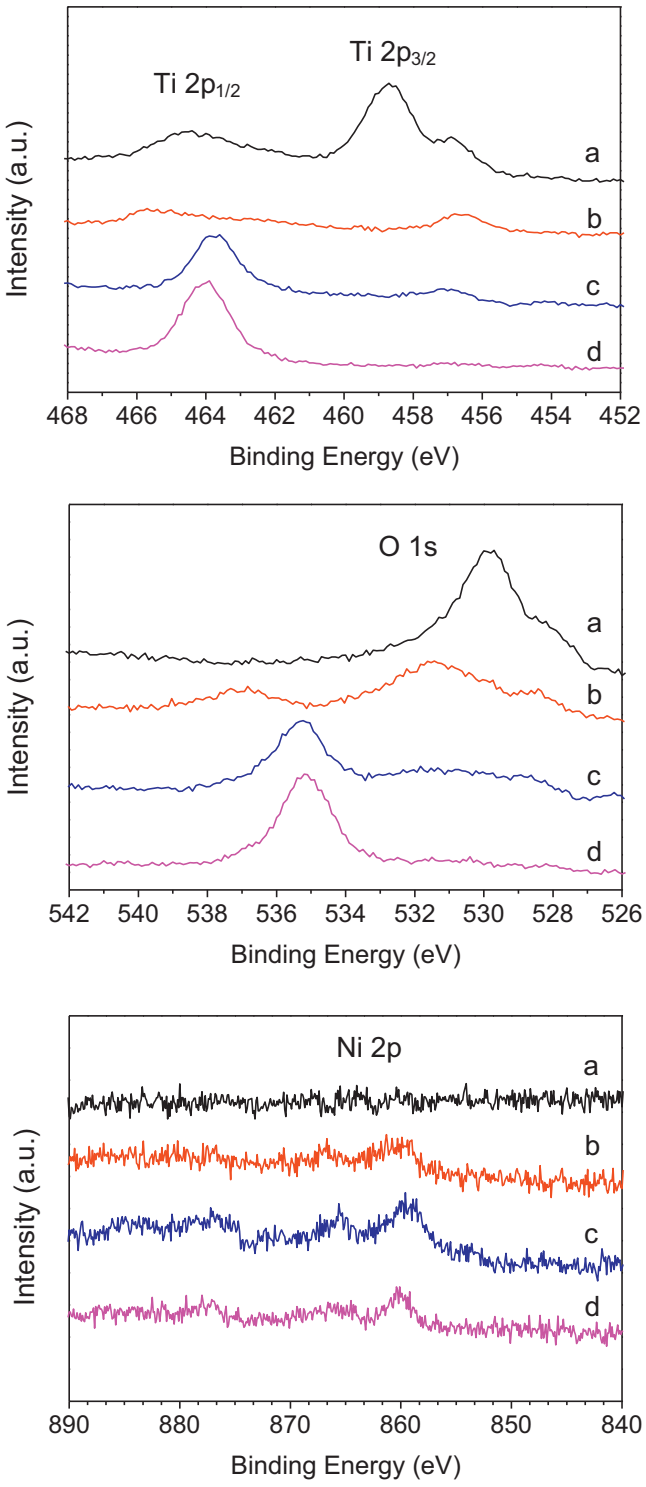

Fig. 5. XPS spectra of Ti 2p, O 1s, and Ni 2p for the NiO_x-unloaded (a) and loaded TiO_2 samples calcined at 250 °C (b), 450 °C (c), and 650 °C (d).

water. The maximum H_2 evolution is obtained with 450 °C calcined NiO_x/TiO_2 sample. However, when the calcination temperature is raised to 650 °C, the surface properties (XPS and UV/vis) are similar to those of the 450 °C calcined sample but the BET surface area is markedly lowered and so this results in a lower activity.

Under the reaction conditions used, the conversion of glycerol was so small that it was difficult to determine its conversion and detect liquid products. These pieces of information may be necessary to make a discussion on reaction mechanisms over NiO_x/TiO_2 catalysts. A few authors discuss the mechanisms of photocatalytic reforming of glycerol over Pt/TiO_2 [5] and CuO_x/TiO_2 [12]. Daskalaki and Kondarides assume that hydroxyl radicals and other oxidants are photogenerated from water and these oxidize and change organic compounds towards lower molecular weight compounds, eventually to CO_2. The photocatalytic reforming of glycerol producing H_2 should occur through those reaction processes. Lalitha et al. also assume several processes for the photocatalytic production of H_2 from glycerol over CuO_x/TiO_2 catalysts [12].

4. Conclusions

NiO_x-loaded TiO_2 catalysts are active for the photocatalytic production of H_2 from aqueous glycerol solution at 50 °C. The activity can remain unchanged in a long time of 12 h at least. The catalytic performance of NiO_x/TiO_2 depends significantly on calcination temperature. The maximum activity can be achieved after the calcination at 450 °C. The calcination temperature would influence the formation of n-type (NiO_x) and p-type (TiO_2) junction. The calcination at 450 °C decreased the band gap energy by 0.58 eV with respect to the mother TiO_2 material, which was responsible for the improved H_2 production. The calcination at a higher temperature of 650 °C caused a significant decrease in the surface area, reducing the catalytic performance.

Acknowledgements

This work was supported by Japan Society for the Promotion of Science (JSPS) with Grant-in-Aid for Scientific Research (B) 22360327 and for JSPS Fellows 2200038601.

References

[1] M. Cargnello, A. Gasparotto, V. Gombac, T. Montini, D. Barreca, P. Fornasiero, European Journal of Inorganic Chemistry (2011) 4309–4323.
[2] K. Shimura, H. Yoshida, Energy & Environmental Sciences 4 (2011) 2467–2481.
[3] R.M. Navarro, M.C. Sánchez-Sáncez, M.C. Alvarez-Galvan, F. del Valle, J.L.G. Fierro, Energy & Environmental Sciences 2 (2009) 35–54.
[4] C.H.C. Zhou, J.N. Beltramini, Y.X. Fan, G.Q.M. Lu, Chemical Society Reviews 37 (2008) 527–549.
[5] V.M. Daskalaki, D.I. Kondarides, Catalysis Today 144 (2009) 75–80.
[6] D.I. Kondarides, V.M. Daskalki, A. Patsoura, X.E. Verykios, Catalysis Letters 122 (2008) 26–32.
[7] N. Fu, G. Lu, Catalysis Letters 127 (2009) 319–322.
[8] N. Luo, Z. Jiang, H. Shi, F. Cao, T. Xiao, P.P. Edwards, International Journal of Hydrogen Energy 34 (2009) 125–129.
[9] M. Bowker, P.R. Davies, L.S. Al-Mazroai, Catalysis Letters 128 (2009) 253–255.
[10] T. Montini, V. Gombac, L. Sordelli, J.J. Delgado, X. Chen, G. Adami, P. Fornasiero, ChemCatChem 3 (2011) 574–577.
[11] V. Gombac, L. Sordelli, T. Montini, J.J. Delgado, A. Adamski, G. Adami, M. Cargnello, S. Bernal, P. Fornasiero, Journal of Physical Chemistry A 114 (2010) 3916–3925.
[12] K. Lalitha, G. Sadanandam, V.D. Kumari, M. Subrahmanyam, B. Sreedhar, N.Y. Hebalkar, Journal of Physical Chemistry C 114 (2010) 22181–22189.
[13] A. Kudo, K. Domen, K. Maruya, T. Onishi, Chemical Physics Letters 133 (1987) 517–519.
[14] L. Ren, Y. Zeng, D. Jiang, Solid State Sciences 12 (2010) 138–143.
[15] C. Chen, C. Liao, K. Hsu, Y. Wu, J.C. Wu, Catalysis Communications 12 (2011) 1307–1310.
[16] A. Iwaszuki, M. Nolan, Q. Jin, M. Fujishima, H. Tada, Journal of Physical Chemistry C 117 (2013) 2709–2718.
[17] C.D. Wagner, W.M. Riggs, L.E. Davis, J.F. Moulder, G.E. Muilenberg (Eds.), Handbook of X-ray Photoelectron Spectroscopy, Perkin-Elmer, Minnesota, USA, 1978.
[18] R. Liu, H. Yoshida, S. Narisawa, S. Fujita, M. Arai, RSC Advances 2 (2012) 8002–8006.
[19] X. Li, L. Shi, D. Wang, Q. Luo, J. An, Journal of Chemical Technology and Biotechnology 87 (2012) 1187–1193.
[20] P.I. Sorantin, K. Schwarz, Inorganic Chemistry 31 (1992) 567–576.
[21] A.L. Linsebigler, G. Lu, J.T. Yates Jr., Chemical Reviews 95 (1995) 735–758.
[22] G. Colón, J.M. Sánchez-España, M.C. Hidalgo, J.A. Navío, Journal of Photochemistry and Photobiology A: Chemistry 179 (2006) 20–27.
[23] T.L. Thompson, J.T. Yates Jr., Chemical Reviews 106 (2006) 4428–4453.
[24] H.P. Klug, L.E. Alexander, X-ray Diffraction Procedures for Polycrystalline and Amorphous Materials, John Wiley, London, UK, 1954, pp. 491.